NeuroImage 108 (2015) 441–449

Contents lists available at ScienceDirect

NeuroImage

journal homepage: www.elsevier.com/locate/ynimg

Waxholm Space atlas of the rat brain hippocampal region: Three-dimensional delineations based on magnetic resonance and diffusion tensor imaging

Lisa J. Kjonigsen [a], Sveinung Lillehaug [a], Jan G. Bjaalie [a], Menno P. Witter [b], Trygve B. Leergaard [a,*]

[a] Institute of Basic Medical Sciences, University of Oslo, Oslo, Norway
[b] Kavli Institute for Systems Neuroscience and Centre for Neural Computation, Norwegian University of Science and Technology, Trondheim, Norway

ARTICLE INFO

Article history:
Accepted 31 December 2014
Available online 10 January 2015

Keywords:
Diffusion tensor imaging
Digital brain atlasing
Hippocampus
Magnetic resonance imaging
Neuroinformatics
Parahippocampus
Segmentation
Sprague Dawley rat
Template
Waxholm Space

ABSTRACT

Atlases of the rat brain are widely used as reference for orientation, planning of experiments, and as tools for assigning location to experimental data. Improved quality and use of magnetic resonance imaging (MRI) and other tomographical imaging techniques in rats have allowed the development of new three-dimensional (3-D) volumetric brain atlas templates. The rat hippocampal region is a commonly used model for basic research on memory and learning, and for preclinical investigations of brain disease. The region features a complex anatomical organization with multiple subdivisions that can be identified on the basis of specific cytoarchitectonic or chemoarchitectonic criteria. We here investigate the extent to which it is possible to identify boundaries of divisions of the hippocampal region on the basis of high-resolution MRI contrast. We present the boundaries of 13 divisions, identified and delineated based on multiple types of image contrast observed in the recently published Waxholm Space MRI/DTI template for the Sprague Dawley rat brain (Papp et al., Neuroimage 97:374–386, 2014). The new detailed delineations of the hippocampal formation and parahippocampal region (Waxholm Space atlas of the Sprague Dawley rat brain, v2.0) are shared via the INCF Software Center (http://software.incf.org/), where also the MRI/DTI reference template is available. The present update of the Waxholm Space atlas of the rat brain is intended to facilitate interpretation, analysis, and integration of experimental data from this anatomically complex region.

Introduction

The hippocampal formation and adjacent parahippocampal areas, together constituting the hippocampal region, are intensively investigated in the rat brain in the context of understanding memory and learning processes (Eichenbaum et al., 2007) and neurological diseases such as Alzheimer's disease and epilepsy (Braak and Braak, 1991; Schwarcz and Witter, 2002). Due to the anatomical complexity of this region, accurate atlas resources are important for planning experiments, conducting analyses, reporting findings, and comparing results across investigations. The hippocampal region is subdivided by interpretation of cyto-, chemo-, and myeloarhitectonic patterns observed in histological materials. Several parcellation schemes are available in the form of atlas diagrams (Swanson, 2004; Paxinos and Watson, 2007), or textual descriptions (e.g. Witter and Amaral, 2004; Andersen et al., 2007; Bota and Swanson, 2010). The currently most detailed and up-to-date accounts of hippocampal parcellation in the rat comprise an interactive web-based resource linking delineated histological images with up-to-date criteria for subdividing the hippocampal region (Kjonigsen et al., 2011), and a comprehensive description of boundaries observed in three standard sectional planes (Boccara et al., 2014).

Improved imaging technologies have given rise to a new generation of three-dimensional (3-D) digital rodent brain atlases, highly relevant for orientation in the hippocampal region. These volumetric brain atlases, based on high resolution magnetic resonance imaging (MRI) templates (Johnson et al., 2010; Bowden et al., 2011; Hawrylycz et al., 2011; Veraart et al., 2011; Papp et al., 2014) provide anatomical reference spaces that are suitable both for 3-D tomographical and two-dimensional (2-D) experimental data, and have the advantage that they can be resliced in arbitrary planes. But, currently available 3-D rat brain atlases lack hippocampal subdivisions, the underlying MRI templates have considerably lower spatial resolution than histological images, and it is unknown whether hippocampal subregions can be identified on the basis of MRI contrast. It was recently demonstrated that combined use of high-resolution structural and diffusion MRI in the Waxholm Space template of the Sprague Dawley rat brain allows delineation of a large number of brain regions (Papp et al., 2014).

We here extend this work to investigate the extent to which subdivisions of the hippocampal region, as defined in our recent accounts (Kjonigsen et al., 2011; Boccara et al., 2014), can be identified in the

* Corresponding author at: Institute of Basic Medical Sciences, University of Oslo, P.O. Box 1105 Blindern, N-0317 Oslo, Norway. Fax: +47 22851278.
E-mail address: t.b.leergaard@medisin.uio.no (T.B. Leergaard).

http://dx.doi.org/10.1016/j.neuroimage.2014.12.080

Waxholm Space MRI template. We present a 3-D atlas of 13 divisions of the hippocampal region with boundaries identified and delineated by use of multiple features observed in structural MRI and diffusion tensor imaging (DTI) data, and interpreted in relation to cyto- and chemoarchitectonic features in stained histological sections. These delineations represent the first major update of the existing Waxholm Space atlas of the Sprague Dawley rat brain (Papp et al., 2014), and are shared via the INCF software center (http://software.incf.org/).

Methods

Waxholm Space template for the rat brain

The present atlas of the hippocampal region was defined in the Waxholm Space MRI/DTI template for the Sprague Dawley brain (version 1.01; Papp et al., 2015), available from the INCF Software Center (http://software.incf.org/software/waxholm-space-atlas-of-the-sprague-dawley-rat-brain). This template comprises microscopic resolution, contrast enhanced MRI/DTI data acquired ex vivo from an adult male Sprague Dawley rat head (age 80 days, weight 397.6 g, Charles River, Wilmington, MA, USA) by use of a 7 *T* small animal MRI system (Magnex Scientific, Yarnton, Oxford, UK) at the Duke Center for In Vivo Microscopy (Durham, NC, USA). The template includes T_2*-weighted gradient recalled echo anatomic images with a Nyquist isotropic spatial resolution of 39 μm, and diffusion tensor datasets acquired with a Nyquist isotropic spatial resolution of 78 μm. Technical details are provided in Papp et al. (2014). The high resolution Waxholm Space MRI/DTI template for the Sprague Dawley rat brain (v1.01; Papp et al., 2015; NIfTII format) was downloaded from the INCF Software Center (http://software.incf.org/software/waxholm-space-atlas-of-the-sprague-dawley-rat-brain). The present delineations were defined using T_2*-weighted MRI, DTI, and fractional anisotropy (FA) maps from the following downloadable files: T2*-weighted MRI template v1.01; Color FA map v1.01; FA map v1.01. The first version of the atlas (Sprague Dawley Atlas v1.01; ITK-SNAP label v1-v1.01) was used as a starting point for the delineations.

Image delineation

Divisions of the hippocampal formation and parahippocampal region were manually delineated using ITK-SNAP software (version 2.4, Yushkevich et al., 2006, www.iktsnap.org). MRI data were viewed in ITK-SNAP using the default 16-bit grayscale color map (black to white); where dark areas in the image correspond to low signal intensity and bright areas correspond to high signal intensity. Neuroanatomical boundaries were delineated on the basis of image contrast observed in T_2*-weighted images and diffusion tensor images (DTI). In T_2*-weighted images, below referred to as structural MRI (sMRI) maps, white matter regions tend to have low signal intensities and appear dark, while gray matter regions generally have higher signal intensities and appear brighter. The DTI color maps show the orientation and magnitude of diffusion occurring at each voxel, with the red, green, and blue (RGB) components of each voxel defined by the primary eigenvector of the diffusion weighted images, and the brightness determined using fractional anisotropy (FA) values computed from the three diffusion eigenvalues after tensor decomposition (for further details, see Papp et al., 2014). FA values are also visualized in grayscale FA maps in which voxel brightness is determined by the degree of anisotropic diffusion. Our objective was to delineate the same structures as previously defined in the histology-based Rat Hippocampus Atlas (Kjonigsen et al., 2011; Boccara et al., 2014). Boundaries were manually delineated on the basis of observable features in the volumetric data, aided by comparison to cyto- and chemoarchitectonic features visible in histological section images from Long Evans rats, available from the online Rat Hippocampus Atlas (Kjonigsen et al., 2011; Boccara et al., 2014), as well as cyto- and myeloarchitectonic features observed in a collection of coronal, sagittal, and horizontal sections from normal adult Sprague Dawley rat brains (T.B. Leergaard and J.G. Bjaalie, unpublished work; see, also Leergaard et al., 2010; White et al., 2013). The left and right hemispheres of the brain were delineated separately. The delineated divisions were color-coded in agreement with recent reports (van Strien et al., 2009; Kjonigsen et al., 2011).

Waxhom Space atlas v2.0

The delineations presented here replace the delineations of the hippocampal formation and parahippocampal region provided in the first release (v1.0/v1.01) of the atlas (Papp et al., 2015). In addition to the updated hippocampal delineations, we have adjusted the delineation of regions bordering on the hippocampus and hippocampus proper. The new delineations are included in the downloadable file “Sprague Dawley Atlas v2.0”. This file includes 79 anatomical structures, of which 13 are the new or revised delineations of the hippocampal formation and parahippocampal region, and 66 structures are delineations from v. 1.01, as described in Papp et al. (2015). Two structures (‘neocortex’ and ‘corpus callosum and associated subcortical white matter’) were adjusted to match the updated outer boundaries of the hippocampal formation and parahippocampal region. The anatomical delineations provided in the present report and corresponding label descriptions are made available through the INCF Software Center (http://software.incf.org/software/waxholm-space-atlas-of-the-sprague-dawley-rat-brain) in formats compatible with ITK-SNAP and the Mouse BIRN Atlasing Toolkit (MBAT, Lee et al., 2010). Volumetric images are provided as standard Neuroimaging Informatics Technology Initiative (NIfTI) files.

Results

We here present a volumetric atlas of the rat hippocampal region defined in a Waxholm Space structural and diffusion weighted MRI template of the Sprague Dawley rat brain (Papp et al., 2014). We have delineated 13 divisions in the hippocampal formation and parahippocampal region on the basis of architectural features observed in sMRI and DTI/FA images, compared to cyto- and chemoarchitectonically defined regions (Kjonigsen et al., 2011; Boccara et al., 2014).

Nomenclature

The hippocampal region comprises the hippocampal formation and the parahippocampal region (Cappaert et al., 2014). The hippocampal formation is a C-shaped structure, positioned posteriorly in the hemisphere of the rat brain (Figs. 1A, A′), bordering on the septal complex dorsally and the amygdaloid complex ventrally. It has the characteristic three layered organization of the allocortex, with a superficial, neuron sparse plexiform layer, a middle, densely packed principal cell layer, and an inner, fibrous polymorph layer (Figs. 1D–F). The hippocampal formation encompasses four main subfields, distributed from proximal to distal along the transverse axis of the hippocampus (Fig. 1A′), with the dentate gyrus as the most medial and proximal portion, laterally flanked by the cornu ammonis (CA) with its three subfields (CA1, CA2, CA3), and the subiculum. The fourth subfield is the fasciola cinereum, which extends medially as a longitudinal continuation of the hippocampal formation (Stephan, 1975). The parahippocampal region (Fig. 1B) includes several interconnected six-layered cortical areas (Figs. 1D–F) that are all reciprocally connected with the hippocampal formation (Cappaert et al., 2014). The parahipocampal areas are the presubiculum, parasubiculum, entorhinal cortex (with a medial and lateral part), perirhinal cortex (including areas 35 and 36), and postrhinal cortex. We employ boundary definitions as outlined in The Rat Hippocampal Atlas (Kjonigsen et al., 2011, www.rbwb.org), that have recently been further detailed for the three main planes

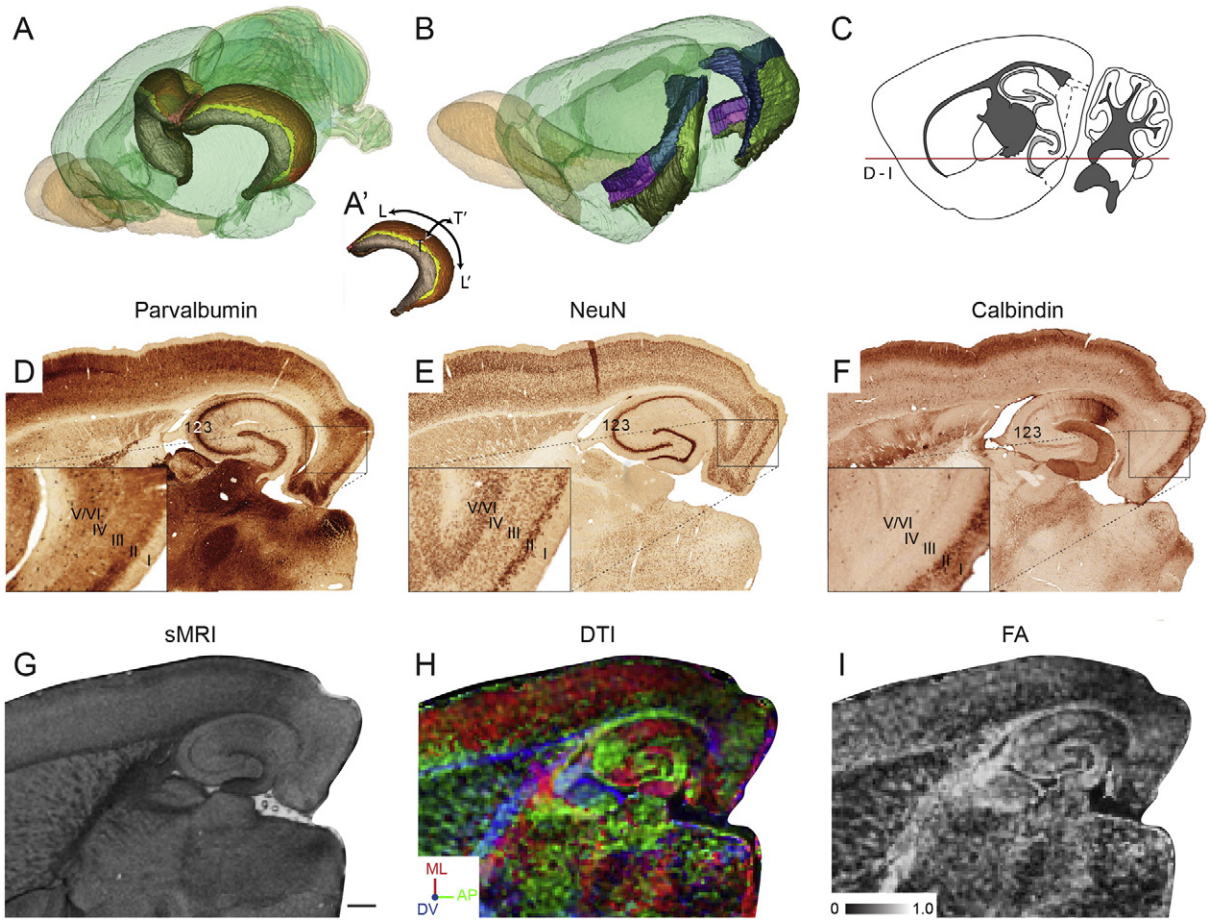

Fig. 1. The hippocampal formation and parahippocampal region. (A,B): Three-dimensional visualizations of the hippocampal formation (A,A′) and the parahippocampal region (B) based on the Waxholm Space Brain Atlas v2.0. (A′): Three-dimensional visualization of the C-shaped hippocampal formation with indication of the long (L-L′) and transverse (T-T′) axis of the hippocampal formation. C) Schematic drawing of a sagittal section, indicating the dorsoventral level of the horizontal sections shown in D–F. (D–F): Images of horizontal histological rat brain sections (data from Boccara et al., 2014), stained for parvalbumin (D), neurons (NeuN, E), and calbindin (F), showing cyto- and chemoarchitectonic features of the hippocampal region. Numbers 1–3 indicate the three layers of the hippocampal formation. Insets in the lower left hand corner show higher power images of the layered (I–VI) organization of the parahippocampal region. (G–I): sMRI, DTI, and FA maps used for anatomical delineations in the atlas, shown in horizontal slices corresponding to D–F. Inset in H shows the RGB color codes for DTI orientations. AP, anteroposterior (green), DV, dorsoventral (blue), and ML, mediolateral (red). Scale bar, 1 mm.

of sectioning using cyto- and chemoarchitectonic criteria (Boccara et al., 2014).

Identification of borders

Anatomical borders were identified on the basis of observed sMRI signal intensities (Fig. 2), regional differences in FA, or DTI orientations (Figs. 1, 3–5). Key features observed in sMRI, DTI, and FA maps are summarized in Table 1. All MRI images were inspected in coronal, sagittal and horizontal slices and interpreted in light of architectonic features observed in histological sections from corresponding levels. Interactive viewing of the MRI data, observing regional features across several levels in multiple planes greatly facilitated the identification of boundaries. Boundaries were related to previously defined histological delineation criteria (Kjonigsen et al., 2011; Boccara et al., 2014). The cell layers of the hippocampal formation and parahippocampal regions were to a variable degree distinguishable in the MRI data (Figs. 1G–I). Although specific architectonic features were variably visible across regions, it was possible to identify nearly all boundaries on the basis of combined observations of MRI contrast, as described below. Only a few boundaries (the ventral part of the boundary between fasciola cinereum and CA1, and the dorsal boundary of the postrhinal cortex, see below) were difficult to identify in the MRI template and were extrapolated from the histological atlas (Kjonigsen et al., 2011; Boccara et al., 2014) using local anatomical landmarks.

The outer borders of the hippocampal region

The boundaries of the hippocampal region with adjacent cortical regions are formed by the border of the entorhinal cortex with the olfactory and periamygdaloid cortex, the perirhinal areas 35 and 36 with the insular cortex, and the perirhinal area 36 and postrhinal cortex with the temporal cortex. The dorsal boundaries of the perirhinal area 36 and dorsal postrhinal cortex towards the temporal and occipital neocortex, were generally identified in sMRI maps by observation of relatively bright layers III and IV in the neocortex (Figs. 2A,E). The neocortex was further characterized by a distinct, dark layer II, which was less prominent in the hippocampal region. These boundaries were also distinguished by a transition from a relatively laminar neocortex to a more homogeneous dorsal perirhinal area 36 in sMRI maps (Figs. 2E,F) and dorsal postrhinal cortex (Figs. 2A,C,F).

The hippocampal formation

Dentate gyrus

The molecular, granule cell, and polymorph layers of the dentate gyrus were clearly visible in the sMRI maps (Figs. 2A–D). The border between the polymorph of the dentate gyrus and the proximal tip of CA3 was identified by a distinct shift to lower sMRI signal intensity

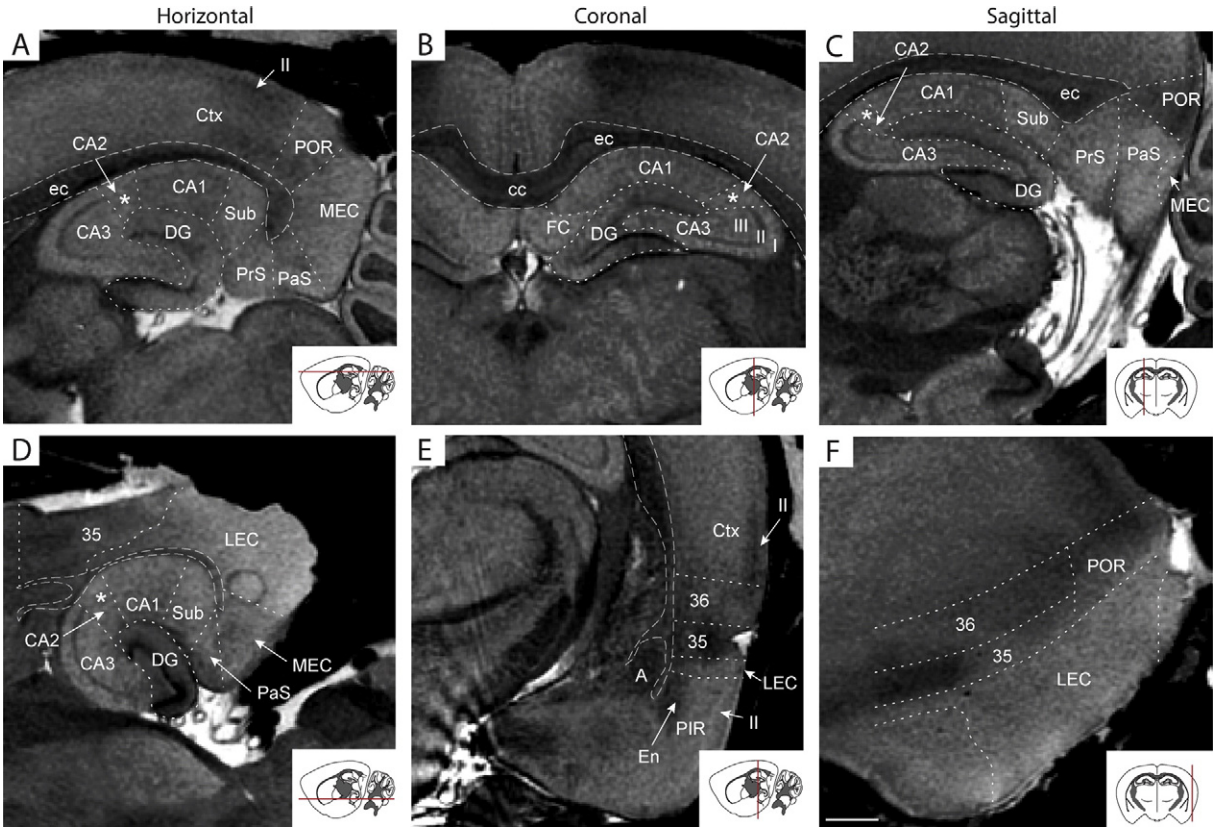

Fig. 2. Structural details visible in T2*-weighted MRI. Selected horizontal (A,D), coronal (B,E), and sagittal (C,F) sMRI slices illustrating key anatomical features observed in the hippocampal formation and parahippocampal region (summarized in Table 1). Inset drawings indicate slice positions in the brain. Dashed lines indicate atlas boundaries. It should be noted that all structural features are best observed by interactive viewing of MRI data across several levels in multiple planes, since they are inconsistently present and difficult to observe in individual images. Asterisk indicates absence of dark layer II in CA2. I, layer 1; II, layer 2; III, layer 3; 35, perirhinal area 35; 36, perirhinal area 36; CA1, cornu ammonis area 1; CA2, cornu ammonis area 2; CA3, cornu ammonis area 3; cc, corpus callosum; Ctx, neocortex; DG, dentate gyrus; ec, external capsule; EC, entorhinal cortex; En, endopiriform nucleus; FC, fasciola cinereum; lateral entorhinal cortex; MEC, medial entorhinal cortex; PaS, parasubiculum; PIR, piriform cortex; POR, postrhinal cortex; PrS, presubiculum; Sub, subiculum. Scale bar, 1 mm.

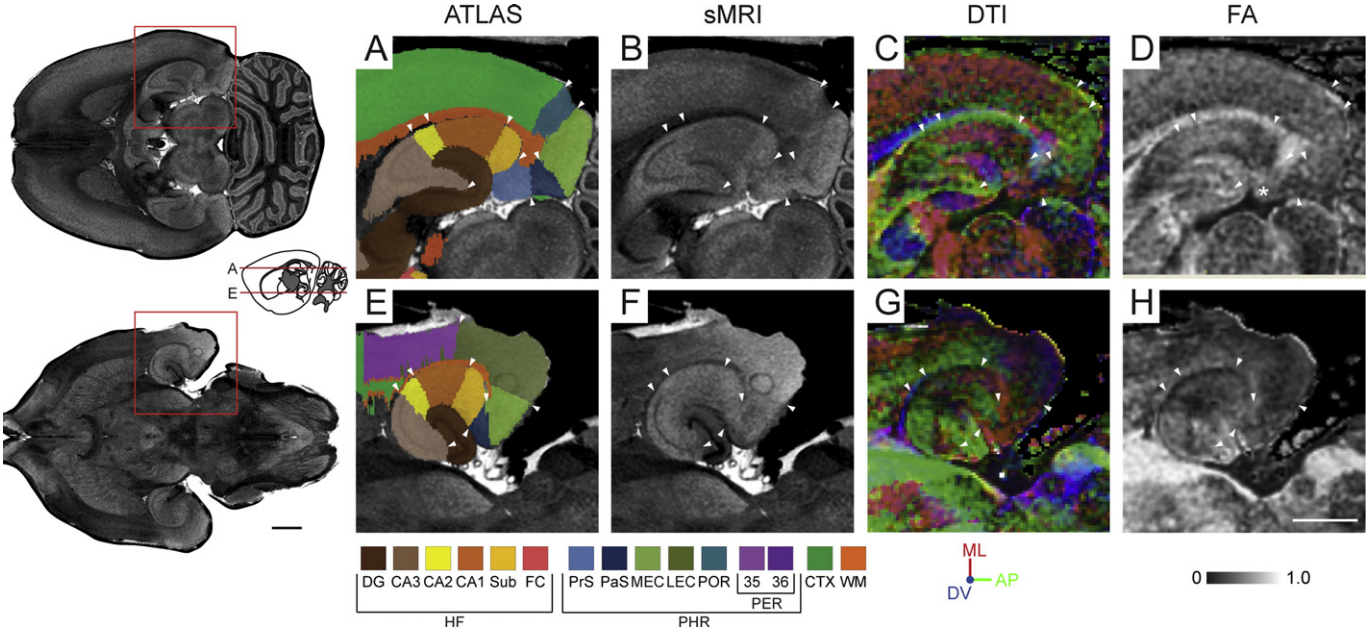

Fig. 3. MRI contrast and atlas delineations in horizontal slices. Anatomical delineations (A,E) and underlying MRI features (B–D, F–H) in the hippocampal formation and parahippocampal region, shown in horizontal MRI slices from two different dorsoventral levels at locations indicated in the insets (left). Inset below panel G shows the RGB color code used for DTI orientation, inset below panel H shows FA grayscale values. Arrowheads indicate corresponding positions across panels A–D and E–H. Asterisk in D indicates the presubiculum, with higher (brighter) FA values than surrounding areas. AP, anteroposterior; CA1, cornu ammonis area 1; CA2, cornu ammonis area 2; CA3, cornu ammonis area 3; CTX, cerebral cortex; DG, dentate gyrus; DV, dorsoventral; FC, fasciola cinereum; HF, hippocampal formation; LEC, lateral enthorhinal cortex; MEC, medial enthorinal cortex; ML, mediolateral; PaS, parasubiculum; PER 35, perirhinal area 35; PER 36, perirhinal area 36; PHR, perihippocampal region; POR, postrhinal cortex; PrS, presubiculum; Sub, subiculum; WM, white matter. Scale bars, 1 mm.

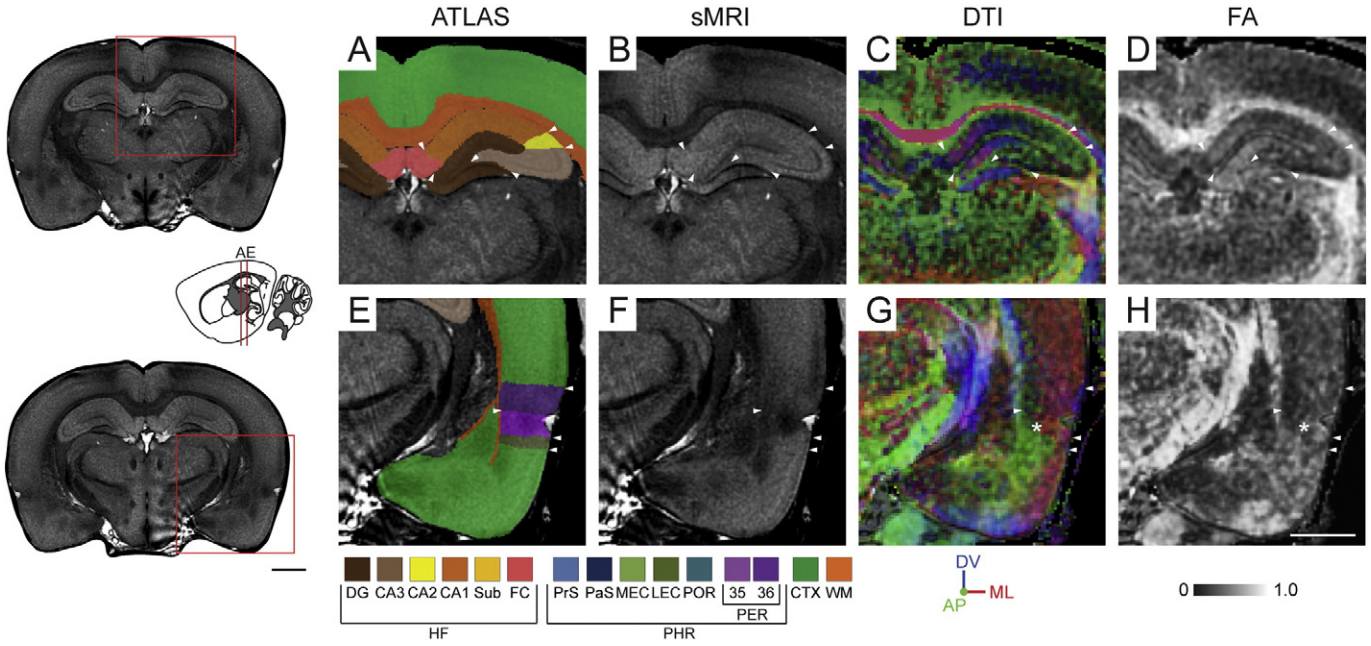

Fig. 4. MRI contrast and atlas delineations in coronal slices. Anatomical delineations (A,E) and underlying MRI features (B–D, F–H) in the hippocampal formation and parahippocampal region, shown in coronal MRI slices from two different anteroposterior levels at locations indicated in the insets (left). Inset below panel G shows the RGB color code used for DTI orientation; inset below panel H shows FA grayscale values. Arrowheads indicate corresponding positions across panels A–D and E–H. The asterisks in G,H indicate the anterior part of area 35, with higher FA values in its superficial layers compared to the surrounding areas. AP, anteroposterior; CA1, cornu ammonis area 1; CA2, cornu ammonis area 2; CA3, cornu ammonis area 3; CTX, cerebral cortex; DG, dentate gyrus; DV, dorsoventral; FC, fasciola cinereum; HF, hippocampal formation; LEC, lateral enthorhinal cortex; MEC, medial enthorinal cortex; ML, mediolateral; PaS, parasubiculum; PER 35, perirhinal area 35; PER 36, perirhinal area 36; PHR, perihippocampal region; POR, postrhinal cortex; PrS, presubiculum; Sub, subiculum; WM, white matter. Scale bars, 1 mm.

(dark) in the dentate gyrus (Figs. 2A–D), spatially corresponding to the transition from the overall calbindin negative cell layer and neuropil of CA3 (except for the mossy fibers) to the calbindin positive dentate gyrus, seen in histological material (Boccara et al., 2014).

Cornu ammonis

The external boundaries of the CA fields towards the subiculum and dentate gyrus were identified by the presence of a distinct cell layer with low sMRI signal intensity (dark) in CA1 and CA3, contrasting

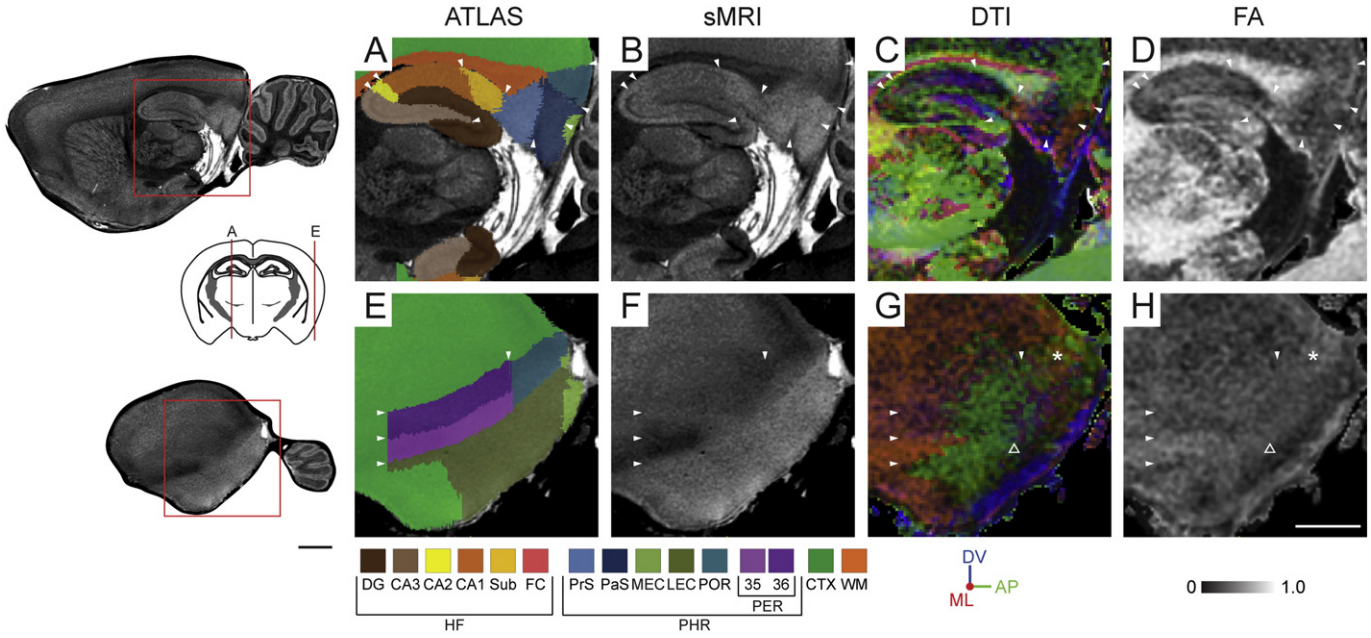

Fig. 5. MRI contrast and atlas delineations in sagittal slices. Anatomical delineations (A,E) and underlying MRI features (B–D, F–H) in the hippocampal formation and parahippocampal region, shown in sagittal MRI slices from two different mediolateral levels at locations indicated in the insets (left). Inset below panel G shows the RGB color code used for DTI orientation; inset below panel H shows FA grayscale values. Arrowheads indicate corresponding positions across panels A–D and E–H. The asterisks in G, H indicate the postrhinal cortex, distinguished by higher (brighter) FA values and somewhat wider cell layers compared to the surrounding areas. The triangles in G, H indicate the distinct laminar appearance in DTI and FA images of the entorhinal cortex. AP, anteroposterior; CA1, cornu ammonis 1; CA2, cornu ammonis 2; CA3, cornu ammonis 3; CTX, cerebral cortex; DG, dentate gyrus; DV, dorsoventral; FC, fasciola cinereum; HF, hippocampal formation; LEC, lateral enthorhinal cortex; MEC, medial enthorinal cortex; ML, mediolateral; PaS, parasubiculum; PER 35, perirhinal area 35; PER 36, perirhinal area 36; PHR, perihippocampal region; POR, postrhinal cortex; PrS, presubiculum; Sub, subiculum; WM, white matter. Scale bars, 1 mm.

Table 1
Key morphological features of areas and borders.

Region name		Key features in structural MRI or DTI/FA maps
Hippocampal formation		
DG	Dentate gyrus	Darker appearance in sMRI than neighboring CA3
CA	Cornu ammonis	Medium dark in sMRI, brighter than DG, darker than SUB, dark cell layer
CA1	Cornu ammonis, area 1	Presence of thin, dark pyramidal cell layer in sMRI
CA2	Cornu ammonis, area 2	Absence of thin, dark pyramidal cell layer in sMRI
CA3	Cornu ammonis, area 3	Presence of thin, dark pyramidal cell layer in sMRI (less prominent than in CA1)
SUB	Subiculum	Brighter appearance in sMRI than surrounding areas
FC	Fasciola cinereum	Presence of narrow dark zone in sMRI at location corresponding to cell layer in DG
Parahippocampal region		
PrS	Presubiculum	Overall higher FA values than surrounding SUB and EC
PaS	Parasubiculum	Appears brighter in sMRI than POR; predominantly mediolateral DTI orientations
EC	Entorhinal cortex	Superficial layers appear brighter than in PaS, PER, POR; appears laminar in DTI
MEC	Entorhinal cortex, medial area	More heterogeneous appearance in sMRI, with narrow bright layer II, and dark layer IV
LEC	Entorhinal cortex, lateral area	More homogeneous appearance than MEC in sMRI, with less distinct layers II and IV
PER	Perirhinal area	Appears darker in sMRI than EC
PER35	Perirhinal area 35	Superficial layers appear darker in sMRI than area 36
PER36	Perirhinal area 36	Appears more homogeneous in sMRI than Ctx
POR	Postrhinal cortex	Darker sMRI appearance, and more anteroposterior DTI orientations than surrounding regions
Other regions		
Ctx	Neocortex	Dark layer II, and bright layers III and IV in sMRI
EP	Endopiriform nucleus	Ellipsoid shaped region appearing dark in sMRI
PIR	Piriform cortex	Sharply defined, bright layer II in sMRI

with the homogenously brighter appearance of the subiculum (lacking a visible cell layer) and the distinctly darker dentate gyrus (Figs. 2A–D). The boundary between CA fields and dentate gyrus was also demarcated in sMRI maps by a thin, dark zone reflecting the thin sheet of white matter lining the hippocampal fissure (Figs. 2A,C,D). The subdivisions of the CA fields were identified in sMRI maps by the distinctly visible pyramidal cell layer, appearing as thin, dark zone in CA1 and CA3, but not in CA2. The discontinuation of the cell layer in CA2 was clearly seen in horizontal and sagittal slices (Figs 2A–D). Histologically, CA2 is identified by its slightly wider principal cell layer (Boccara et al., 2014), but this difference could not be observed in the MRI data.

Subiculum

The subiculum was characterized by its distinctly brighter appearance in sMRI, relative to the surrounding cornu ammonis and presubiculum, and the absence of a dark pyramidal layer (Figs. 2A,C,D). The principal cell layer of the subiculum, which in histological material is characterized by lower cell densities and absence of calbindin staining (Boccara et al., 2014), could not be distinguished.

Fasciola cinereum

The fasciola cinereum is a small medial extension of the most anterior part of the hippocampus which is readily distinguished in histological material. In sMRI maps, the fasciola cinereum was distinguished from the dentate gyrus by observing a narrow dark zone at a location corresponding to the principal granule cell layer of the dentate gyrus (Fig. 2B). The dorsal part of the border between fasciola cinereum and CA1 was in coronal sMRI slices visible as a thin, dark rim reflecting the white matter of the alveus curving around the medial aspect of CA1 (Fig. 2B).

The parahippocampal region

Presubiculum and parasubiculum

The presubiculum and parasubiculum are intercalated between the subiculum and entorhinal cortex (Fig. 2D). The presubiculum was differentiated from the subiculum and parasubiculum on the basis of the distinctly higher FA values in this region (Fig. 3D; asterisk). The boundary between the parasubiculum and entorhinal cortex was identified by a thin rim of low sMRI signal intensity (dark), reflecting white matter, extending towards the pial surface as an extension of the lamina dissecans and alveus (Figs. 2A,C). At its dorsolateral extreme, the parasubiculum was distinguished from the postrhinal cortex on the basis of higher MRI signal intensity (bright) in the parasubiculum (Fig. 2C), and further by a preponderance of mediolateral (red DTI color) diffusion orientations in the parasubiculum (Fig. 5C), contrasting the anteroposterior (green DTI color) diffusion orientations (Fig. 5C) observed in the middle layers of the postrhinal cortex.

Entorhinal cortex

The entorhinal cortex was readily distinguished from the surrounding parasubiculum, perirhinal and postrhinal cortices in sMRI maps (Figs. 2A,D), by the presence of distinctly brighter superficial layers and a thin dark layer, faintly indicating the lamina dissecans (a cell free layer IV containing afferent and efferent fibers which is present in the entorhinal cortex, and to a lesser extent also in the presubiculum and parasubiculum). The entorhinal cortex was further characterized by a more distinct laminar appearance in DTI and FA maps (Figs. 5G,H). The boundary between the entorhinal cortex and the postrhinal cortex was detected on the basis of the relatively brighter appearance of the entorhinal cortex in sMRI maps, as well as by the presence of anteroposterior orientations in DTI maps (Figs. 6G,H), reflecting the anteroposteriorly oriented intrinsic fibers of the entorhinal cortex (Dolorfo and Amaral, 1998). At the border between the entorhinal cortex and the anteroventrally located piriform cortex, layer II (here appearing bright in sMRI maps) was more sharply defined in the piriform cortex, and more blurred in the entorhinal cortex (Fig. 2E). This boundary was also indicated by the presence of the endopiriform nucleus (Fig. 2E), underlying the piriform cortex, visible as an ellipsoid region with low sMRI signal intensity (dark), located close to the white matter of the external capsule (opposed to the amygdala, Fig. 2E). In horizontal slices, the point where the lamina dissecans curved sharply towards the medial pial surface defined the medial edge of the entorhinal cortex and its boundary with the parasubiculum (Fig. 2A). In horizontal sMRI maps, the medial entorhinal cortex was distinguished from the lateral entorhinal cortex (Fig. 2D) by the relatively more heterogeneous aspect, the presence of a narrow, bright layer II, and a dark layer IV (lamina dissecans) in medial entorhinal cortex (Figs. 2A,D). This difference was much harder to see in the coronal and sagittal planes. Further subdivisions of the entorhinal cortex (Insausti et al., 1997; Kjonigsen et al., 2011; Boccara et al., 2014) could not be consistently identified in the MR images, although

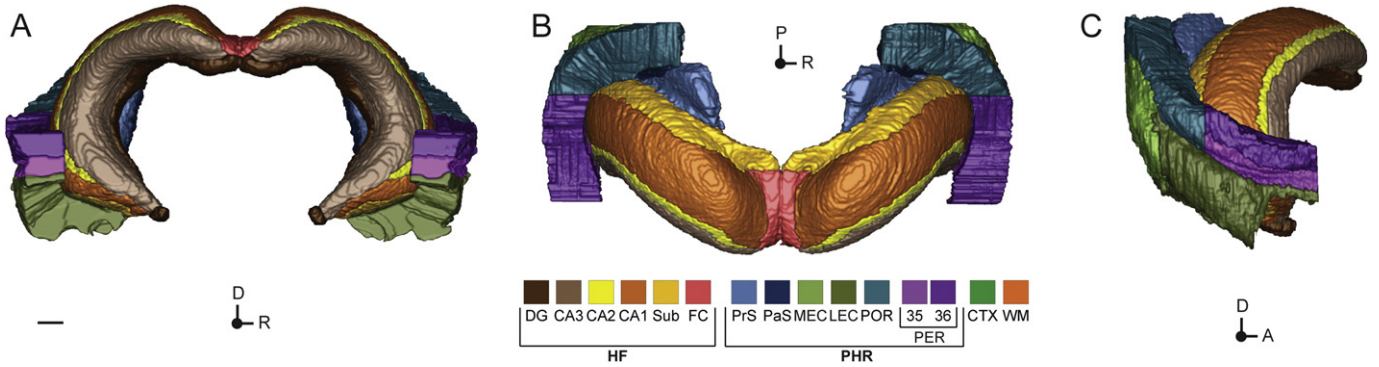

Fig. 6. 3-D views of the hippocampal region. Color coded surface models of the delineations of the hippocampal region, in view from an anterior (A), dorsal (B), and left position (C), corresponding to the standard coronal, horizontal, and sagittal planes used in histology. The 3-D model shows the complex spatial relationships among the different parts constituting the hippocampal region. A, anterior; CA1, cornu ammonis 1; CA2, cornu ammonis 2; CA3, cornu ammonis 3; CTX, cerebral cortex; D, dorsal; DG, dentate gyrus; FC, fasciola cinereum; L, lateral; LEC, lateral enthorhinal cortex; MEC, medial enthorinal cortex; P, posterior; PaS, parasubiculum; PER 35, perirhinal area 35; PER 36, perirhinal area 36; POR, postrhinal cortex; PrS, presubiculum; Sub, subiculum; WM, white matter. Scale bar: 1 mm.

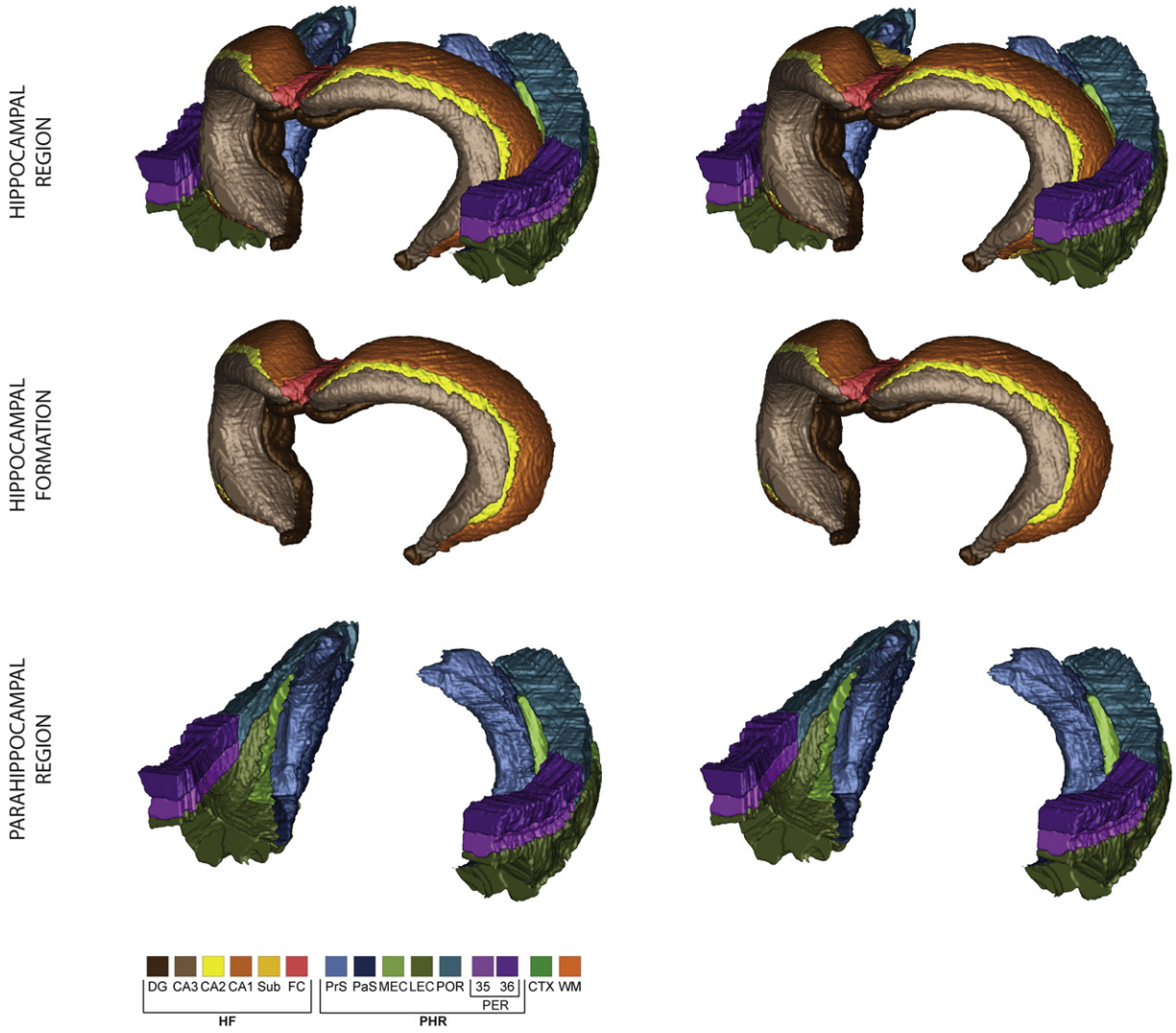

Fig. 7. Stereo images of surface model of the hippocampal formation and parahippocampal region. Stereo image pairs showing the color coded 3-D surface model of the delineations of the hippocampal formation and parahippocampal region, in an oblique view from anterior and left, with separate panels for the hippocampal formation and parahippocampal region. The viewer must cross the eye axes to let the pair of images merge into a 3-D image. A, anterior; CA1, cornu ammonis 1; CA2, cornu ammonis 2; CA3, cornu ammonis 3; CTX, cerebral cortex; D, dorsal; DG, dentate gyrus; FC, fasciola cinereum; L, lateral; LEC, lateral enthorhinal cortex; MEC, medial enthorinal cortex; P, posterior; PaS, parasubiculum; PER 35, perirhinal area 35; PER 36, perirhinal area 36; POR, postrhinal cortex; PrS, presubiculum; Sub, subiculum; WM, white matter. Scale bar: 1 mm.

at some levels it was noted that the caudal entorhinal area appeared brighter in sMRI maps than the ventral intermediate area, while the medial entorhinal area appeared darker and also featured high FA values.

Perirhinal and postrhinal cortices

The border between the perirhinal areas 35 and 36 was identified on the basis of relatively higher FA values in the superficial parts of the anterior area 35 (Fig. 5H, bright FA signal), and distinctly higher sMRI signal intensities (bright) in the superficial layers of area 35 compared to area 36 (Figs. 2E,F). Area 36 was distinguished by a less clear lamination pattern, and a brighter appearance of superficial layers in sMRI maps, relative to the adjacent cortex. The border between area 35 and the (dorsolateral) entorhinal cortex was identified by the characteristic brighter appearance of the entorhinal cortex in sMRI maps, and higher FA values in area 35 (Figs. 4E–H). The border between the perirhinal and postrhinal cortex was difficult to determine in coronal images due to the gradual transition of sMRI signal intensity across these regions, but could be determined in sagittal slices by presence of higher FA values and somewhat wider appearance of the cell layers of the postrhinal cortex (Figs. 5G,H). The border between the postrhinal and entorhinal cortex was readily defined on the basis of lower sMRI signal intensities (dark) and higher FA values in the postrhinal cortex, as well as the more laminar appearance of the entorhinal cortex in FA and DTI maps (Figs. 5G,H).

The three-dimensional shape of the hippocampal region

Computerized surface models of the volumetric delineations of the hippocampal region (Figs. 6, 7) allowed interactive inspection and study of the complex spatial architecture and spatial relationships of these structures. We found the surface models to be helpful for understanding the complex anatomy, both for new students of hippocampal anatomy as well as for experienced researchers interpreting and analyzing experimental data from the region. In our hands, the interactive 3-D model, combined with the option to simultaneously navigate in the three main orientation planes, coronal, horizontal and sagittal, was very useful for the interpretation and delineation of multiplane histological material from this region. This advantage was particularly noticeable when analyzing sections obtained very close and parallel to the cortical surface of the hemisphere (Boccara et al., 2014).

Discussion

We have described detailed MRI/DTI delineations of 13 divisions of the hippocampal region on the basis of observations made in the Waxholm Space MRI/DTI template for the Sprague Dawley rat brain, and provided descriptions of the criteria used to identify the boundaries. Our delineations cover most of the boundaries defined in our histology-based descriptions (Kjonigsen et al., 2011; Boccara et al., 2014). Two boundaries (the ventral part of the boundary between fasciola cinereum and CA1 and the boundary between the perirhinal and temporal cortex) could not be consistently identified in the MRI/DTI data and were extrapolated from the histological atlas using nearby anatomical landmarks. Further, the subareas of the medial and lateral entorhinal cortex (the caudal and medial area of the medial entorhinal cortex, and dorsolateral, dorsal-intermediate, and ventral intermediate areas of the lateral entorhinal cortex (Insausti et al., 1997) could not be distinguished in the MRI/DTI data, and were not delineated. The delineations provided are shared via the INCF software center, constituting an open access resource suitable for 3-D navigation, localization and verification of the spatial properties of the region.

Overall, the MRI/DTI based borders corresponded surprisingly well with the shape and spatial properties of the histologically defined boundaries. It should, however, be noted that boundary features were not consistently visible across entire regions, but involved combined observations of different features reflecting the underlying architectural organization of the tissue, including presence or absence of specific layers, characteristic anatomical shapes, and overall signal homogeneity or heterogeneity.

The present 3-D atlas of the rat hippocampal region is defined within an adult Sprague Dawley brain template, but comparisons with histological data from other strains (Long Evans and Wistar; Kjonigsen et al., 2011; Boccara et al., 2014) indicate that the region is remarkably consistent across species. We are therefore confident that the employed delineation criteria can be applied to MRI data from other species, provided that corresponding spatial resolution and contrast is used. Further work is needed to increase our understanding of how MRI contrast correlates to histological measures. Also, since the Waxholm Space reference template currently is based on a single subject, it is not known whether all boundaries described here can be identified in population-averaged MRI templates, where subtle structural details could be less conspicuous due to minor intersubject variations, and local misalignment inaccuracies (Veraart et al., 2011). Nevertheless, we believe the current delineations will represent a useful starting point for future exploration of intersubject variability and development of population-averaged atlas templates.

Future efforts may include delineations of the cortical layers, which to a considerable extent are possible to identify in the MRI/DTI template, and to add boundaries that are not visible in the atlas template, either by geometrical transfer from histological atlases, or by enriching the template with additional image modalities. Future enrichment of the atlas template with experimental data may open for delineations based on alternative criteria, such as hodology. Also, since the hippocampal region in of the mouse brain to a large extent is comparable with the rat brain (Witter, 2012) the delineation criteria presented here can probably also be applied to the Waxholm Space mouse brain template (Johnson et al., 2010; Hawrylycz et al., 2011).

Acknowledgments

We thank the INCF committee on digital brain atlasing, Eszter A. Papp and Charlotte N. Boccara for valuable discussions, and Dmitri Darine, and Gergely Csúcs for expert technical assistance. This work was supported by The Research Council of Norway (181676, equipment grant to MPW), the European Commision, FP7-ICT, The Human Brain Project (604102 to JGB), the Norwegian Node of the International Neuroinformatics Coordinating Facility (INCF), and Uninett Sigma.

References

Andersen, P., Morris, R., Amaral, D., Bliss, T., O'Keefe, J., 2007. The Hippocampus Book. Oxford University Press, Oxford.

Boccara, C.N., Kjonigsen, L.J., Hammer, I., Bjaalie, J.G., Leergaard, T.B., Witter, M.P., 2014. A three-plane architectonic atlas of the rat hippocampal region. Hippocampus http://dx.doi.org/10.1002/hipo.22407.

Bota, M., Swanson, L.W., 2010. Collating and curating neuroanatomical nomenclatures: principles and use of the Brain Architecture Knowledge Management System (BAMS). Front. Neuroinform. 4, 3.

Bowden, D.M., Johnson, G.A., Zaborsky, L., Green, W.D.K., Moore, E., Badea, A., Dubach, M.F., Bookstein, F.L., 2011. A symmetrical Waxholm canonical mouse brain for NeuroMaps. J. Neurosci. Methods 195, 170–175.

Braak, H., Braak, E., 1991. Neuropathological stageing of Alzheimer-related changes. Acta Neuropathol. 82, 239–259.

Cappaert, N.L.M., van Strien, N.M., Witter, M.P., 2014. Hippocampal Formation. In: Paxinos, G. (Ed.), The Rat Brain. Elsevier Academic Press, San Diego, CA, US, London, UK, pp. 511–574.

Dolorfo, C.L., Amaral, D.G., 1998. Entorhinal cortex of the rat: organization of intrinsic connections. J. Comp. Neurol. 398, 49–82.

Eichenbaum, H., Yonelinas, A.P., Ranganath, C., 2007. The medial temporal lobe and recognition memory. Annu. Rev. Neurosci. 30, 123–152.

Hawrylycz, M., Baldock, R.A., Burger, A., Hashikawa, T., Johnson, G.A., Martone, M., Ng, L., Lau, C., Larson, S.D., Nissanov, J., Puelles, L., Ruffins, S., Verbeek, F., Zaslavsky, I., Boline, J., 2011. Digital atlasing and standardization in the mouse brain. PLoS Comput. Biol. 7, e1001065.

Insausti, R., Herrero, M.T., Witter, M.P., 1997. Entorhinal cortex of the rat: cytoarchitectonic subdivisions and the origin and distribution of cortical efferents. Hippocampus 7, 146–183.

Johnson, G.A., Badea, A., Brandenburg, J., Cofer, G., Fubara, B., Liu, S., Nissanov, J., 2010. Waxholm space: an image-based reference for coordinating mouse brain research. NeuroImage 53, 365–372.
Kjonigsen, L.J., Leergaard, T.B., Witter, M.P., Bjaalie, J.G., 2011. Digital atlas of anatomical subdivisions and boundaries of the rat hippocampal region. Front. Neuroinform. 5, 2.
Lee, D., Ruffins, S., Ng, Q., Sane, N., Anderson, S., Toga, A., 2010. MBAT: a scalable informatics system for unifying digital atlasing workflows. BMC Bioinform. 11, 608.
Leergaard, T.B., White, N.S., de Crespigny, A., Bolstad, I., D'Arceuil, H., Bjaalie, J.G., Dale, A.M., 2010. Quantitative histological validation of diffusion MRI fiber orientation distributions in the rat brain. PLoS One 5, e8595.
Papp, E.A., Leergaard, T.B., Calabrese, E., Johnson, G.A., Bjaalie, J.G., 2014. Waxholm Space atlas of the Sprague Dawley rat brain. NeuroImage 97, 374–386.
Papp, E.A., Leergaard, T.B., Calabrese, E., Johnson, G.A., Bjaalie, J.G., 2015. Addendum to "Waxholm Space atlas of the Sprague Dawley rat brain" [NeuroImage 97 (2014) 374-386]. NeuroImage 105, 561–562.
Paxinos, G., Watson, C., 2007. The Rat Brain in Stereotaxic Coordinates. Elsevier, Amsterdam; Boston.
Schwarcz, R., Witter, M.P., 2002. Memory impairment in temporal lobe epilepsy: the role of entorhinal lesions. Epilepsy Res. 50, 161–177.
Stephan, H., 1975. Allocortex (Vol. 9). Springer, Berlin.
Swanson, L.W., 2004. Brain Maps: Structure of the Rat Brain. 3rd ed. Academic, Oxford.
van Strien, N.M., Cappaert, N.L., Witter, M.P., 2009. The anatomy of memory: an interactive overview of the parahippocampal–hippocampal network. Nat. Rev. Neurosci. 10, 272–282.
Veraart, J., Leergaard, T.B., Antonsen, B.T., Van Hecke, W., Blockx, I., Jeurissen, B., Jiang, Y., Van der Linden, A., Johnson, G.A., Verhoye, M., Sijbers, J., 2011. Population-averaged diffusion tensor imaging atlas of the Sprague Dawley rat brain. NeuroImage 58, 975–983.
White, N.S., Leergaard, T.B., D'Arceuil, H., Bjaalie, J.G., Dale, A.M., 2013. Probing tissue microstructure with restriction spectrum imaging: histological and theoretical validation. Hum. Brain Mapp. 34, 327–346.
Witter, M.P., 2012. Hippocampus. In: Watson, C., Paxinos, G., Puelles, L. (Eds.), The Mouse Nervous System. Elsevier, Amsterdam, pp. 112–139.
Witter, M.P., Amaral, D.G., 2004. Hippocampal Formation. In: Paxinos, G. (Ed.), The Rat Nervous System. Elsevier, Amsterdam, pp. 637–703.
Yushkevich, P.A., Piven, J., Hazlett, H.C., Smith, R.G., Ho, S., Gee, J.C., Gerig, G., 2006. User-guided 3D active contour segmentation of anatomical structures: significantly improved efficiency and reliability. NeuroImage 31, 1116–1128.